SEM Image Analysis for Quality Control of Nanoparticles

Conference Paper · September 2009

DOI: 10.1007/978-3-642-03767-2_72 · Source: DBLP

SEM Image Analysis for Quality Control of Nanoparticles

S.K. Alexander[1], R. Azencott[1], B.G. Bodmann[1], A. Bouamrani[2], C. Chiappini[2], M. Ferrari[2], X. Liu[2], and E. Tasciotti[2]

[1] Department of Mathematics, University of Houston, Houston TX 77004
simon@math.uh.edu, razencot@math.uh.edu
[2] Biomedical Engineering/NanoMedicine, University of Texas, Houston, TX, 77003

Abstract. In nano-medicine, mesoporous silicon particles provide efficient vehicles for the dissemination and delivery of key proteins at the micron scale. We propose a new quality-control method for the nanopore structure of these particles, based on image analysis software developed to automatically inspect scanning electronic microscopy (SEM) images of nanoparticles in a fully automated fashion. Our algorithm first identifies the precise position and shape of each nanopore, then generates a graphic display of these nanopores and of their boundaries. This is essentially a texture segmentation task, and a key quality-control requirement is fast computing speed. Our software then computes key shape characteristics of individual nanopores, such as area, outer diameter, eccentricity, etc., and then generates means, standard deviations, and histograms of each pore-shape feature. Thus, the image analysis algorithms automatically produce a vector from each image which contains relevant nanoparticle quality control characteristics, either for comparison to pre-established acceptability thresholds, or for the analysis of homogeneity and the detection of outliers among families of nanoparticles.

1 SEM Image Data and Quality Control Targets

Quality control in the production of nanostructures poses a challenge for image processing, because it requires interpreting high-resolution images which may be plagued by substantial amounts of noise of various characteristics, and because the material is by design heterogeneous and thus requires flexible analysis algorithms. We present new algorithms for SEM images analysis focused on quality control of porous silicon (pSi) and associated microparticles (PSMs).

Visual inspection of nanoparticles is performed on 24bit SEM images typically of size 1024×768. Each nanoparticle occupies an image surface of approximately 500×500 pixels, has dimensions of the order of 3×3 microns and gathers between 500 and 1000 nanopores having similar shapes. The main goal of our algorithmic image analysis is first to identify the precise positions and shapes of each nanopore and its boundary in a fully automated fashion, and generate a graphic display of these nanopores and boundaries. This is essentially a texture segmentation task, and a key quality control requirement is fast computing

X. Jiang and N. Petkov (Eds.): CAIP 2009, LNCS 5702, pp. 590–597, 2009.

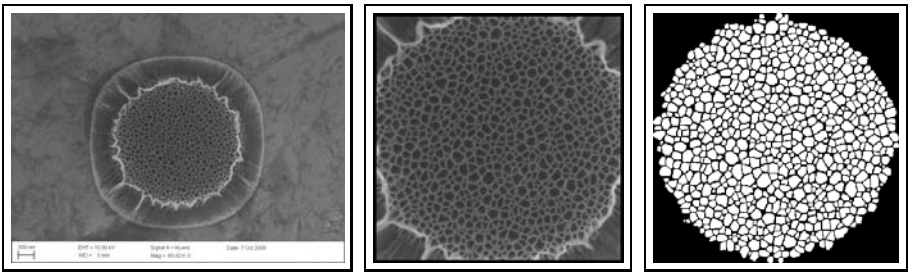

(a) SEM Image **(b)** Region of Interest **(c)** Segmented Pores

Fig. 1. Example nanoparticle AN24-GP-12

speed. Then a second algorithm automatically analyzes the shapes of the detected nanopores in order to compute key shape characteristics of nanopores, such as area, outer diameter, eccentricity, boundary thickness, etc.); we thus generate for each nanoparticle a database of roughly 500 to 1000 vectors of individual pore features. At the level of each nanoparticle, we then launch automatic extraction of statistical characteristics of this database, to compute the means, standard deviations, and histograms of each type of shape feature. This defines a vector of nanoparticle characteristics, which thus provides very natural quality control features, either for comparison to pre-established acceptability thresholds, or to analyze homogeneity and outliers among families of nanoparticles.

2 Porous Silicon Microparticles and Nanomedicine Applications

Since the initial proof of its biocompatibility [1] porous silicon has been actively researched as a biomaterial[2,3,4,5,6]. Porous silicon microparticles (PSMs) have demonstrated their efficacy as delivery vectors for therapeutics. PSMs obtained by sonication or ball milling of pSi layers successfully acted as loading and release agents for different drug molecules, encompassing a wide spectrum of solubility and acid/base characteristics[7]. Proteins were also successfully loaded and released from PSM[8]. Oral delivery of pSi has been proven safe[9] and paracellular drug delivery by means of PSMs has been demonstrated in vitro [10]. However, the size and shape polydispersion of PSMs obtained by sonication or ball milling forbids their use as vascular delivery systems. Our group has successfully developed a strategy based on mathematical models [11,12,13], to produce monodisperse porous silicon microparticles of tailored pore size, shape, and porosity (porous silicon elements, PSEs)[14]. We have proven short term safety of PSEs upon injection [15], and demonstrated their suitability as primary vectors in a multi-stage delivery system [16]. The porous silicon elements are produced in a silicon fabrication environment using a top-down approach resulting in selective porosification of bulk silicon wafers. The fabrication process involves multiple

steps: thin film deposition, photolithography, selective dry etch, electrochemical etch, etc. The process is subject to batch-to-batch variations that may influence the final product. Variations in lithographic steps may lead to a different PSE size or shape, and hence to variation of pore size and porosity. But to guarantee the PSEs efficacy as primary delivery vectors, their size, shape, and pore sizes must be reproduced within stringent limits to avoid modifying their flow and margination characteristics , altering the payload biodistribution and release profile due to different diffusion characteristics [17] and pSi degradation kinetics [16]. Currently, quality assessment for PSEs is a two step process. Initially a statistically relevant sample of particles from a single production lot is analyzed by expert interactive measurements on SEM images to assess size and shape uniformity. Secondly ten or more production lots are joined to obtain the minimum 10mg sample size necessary for nitrogen absorption/desorption analysis of pore size and porosity. This latter step risks rejection of good quality lots (representing significant time and resources spent) due to necessarily mixing with other lots. The alternative software based algorithmic image analysis we propose here for quality control of PSEs is much faster and generates robust quantitative evaluations of pore sizes and shapes.

3 Image Analysis

3.1 Algorithmic Outline

We first process a high resolution SEM image (e.g. Figure 1a) to compute a graphic display of pore locations, which may, when required by the user, be spatially restricted to circular bands within the nanoparticle. Below are our main algorithmic steps :

- **Step 1:** ***ROI extraction*** We isolate the nanoparticle of interest, by centering on a region of interest (ROI) labeled I_0. This step is still interactive, but will be easily automatized within a future quality control software. The SEM image as seen in Figure 1a is then cropped, resulting in Figure 1b, and masked to a subimage I_0.
- **Step 2:** ***Histogram equalization*** We compute the intensity histograms H_1, H_2, ..., on small overlapping image patches of identical sizes R_1, R_2, ..., covering our ROI. Local intensities are then distorted nonlinearly in order to equalize and requantize all local histograms H_1, H_2, ... This step generates an image with more uniform distributions of intensities depicted in Figure 2b.
- **Step 3:** ***Pore segmentation*** A number of morphological and statistical operations are performed to isolate the individual nanopores within the ROI. This key segmentation algorithm is detailed below.
- **Step 4:** ***Extraction of pore features*** Following segmentation, each individual pore and its boundary are determined as associated subregions of the ROI image. Classical shape analysis techniques are applied to each one of these subregions in order to compute, for each pore, its area, perimeter,

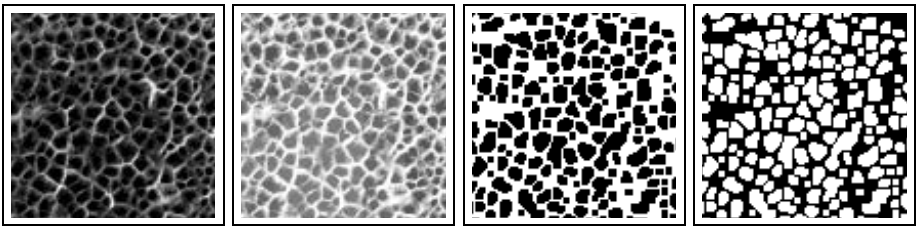

(a) ROI detail **(b)** Processed detail **(c)** Final Boundary **(d)** Pore mask

Fig. 2. Pore shape localization: A detail from the middle of an ROI is shown in (a). The ROI is locally equalized and re-quantized based (b), the pore boundaries are found (c) and finally a mask geometrically identifying all individual pores is created (d).

outer diameter, and boundary thickness, and to evaluate the degree of elongation of the pore, modeled by the eccentricity of an elliptic shape fitted to the pore.

– **Step 5:** ***Nanoparticle quality control features*** Within the approximately circular nanoparticle, we analyze shape features statistics for all pores, computing the mean, standard deviation, and histogram of each pore shape feature extracted at step 4. This process can be carried out globally for each particle, or repeated for only those pores situated within concentric rings of user selected radius. Thus on each circular ring, the characteristics may be compared giving us the ability to perform both inter- and intra-pore comparisons. Furthermore, the cumulative statistics from one set of particles may be compared with those of another set, as appropriate.

3.2 Segmenting the Nanopores

Our *pore segmentation* algorithm is deliberately localized to better to variations in pore depths, pore shapes, and boundary wall thicknesses. This adaptivity lead us below to implement spatially variable morphological operators, as in [18]. We begin with an image subpatch of the raw ROI I_0, as in Figure 2a, which is then broken into overlapping square regions R_j (with dimensions roughly equal to 30×30 pixels in the cases shown here, determined by a rough estimate of pore size set to be a box of 3 times the typical pore diameter, which will vary with resolution and physical pore size). These regions are histogram equalized and requantized, then merged into a single image I_1 (e.g. Figure 2b).

On each region R_j of I_1 the "skeleton" of R_j is computed relative to the median (local to R_j), computed by a morphological algorithm [19]. Note that due to localized equalization processing, the merged skeleton of I_1 does not suffer from intensity fluctuations present in the original image. We then automatically bridge each skeleton gap between the neighboring ends of any two skeleton branches that are not 4-connected. This extended skeleton is then refined by removing spurs and isolated pixels. The final skeleton is then used to mask I_1

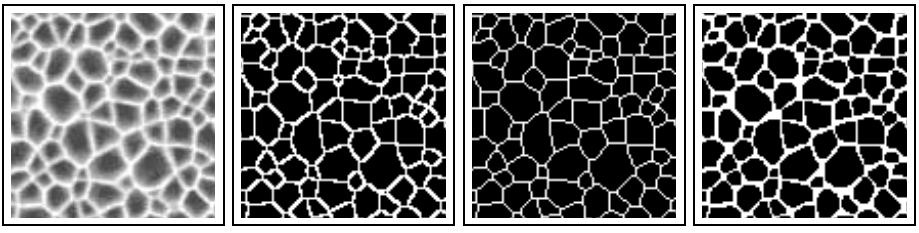

(a) Region **(b)** Initial Skeleton **(c)** Refined Skeleton **(d)** Boundary

Fig. 3. Pore Segmentation steps: (a) locally processed region has (b) initial skeleton which leads to (c) refined skeleton used to find *local intensity threshold* yielding (d) boundary. Finally, the pores are defined as connected components separated by this boundary, as in Figure 2d.

and we compute the mean and standard deviation μ_{skel}, σ_{skel} of pixel intensities over the final skeleton $skel_j$. These values are used to compute a well adapted *local intensity threshold* thr_j on R_j separating intensity values within pores from those on pore boundaries. Using $skel_j$ and thr_j to compute a first version of pore boundaries in R_j, we generate a first map of all pore boundaries (e.g. Figure 2c). This pore boundaries map PB is then cleaned of spurious pixels, and each connected component of $I_1 - PB$ is identified with an individual pore; this defines the final pore map (e.g. Figure 2d). Figure 3 shows details of the skeletonization process and boundary definition on a particularly clear case. The region shown is much larger than R_j boundaries, demonstrating that appropriate partitioning has been performed and does not introduce boundary artifacts.

4 Experimental Results

After a nanoparticle has been processed with the pore segmentation algorithm, the resulting pore map is automatically analyzed as described above in Step 4 to compute a vector of shape features for each pore. An automated statistical analysis of this family of 500 to 1000 vectors of pore shape features computes means and standard deviations of these feature vectors to generate and display a vector of mean quality-control characteristics for the nanoparticle just analyzed.

Our goal was to prove feasibility of software based automated quality control to efficiently monitor the production of nanoparticles, as well as to enable rigorous quantified descriptions of the nanoparticles pore structure. First, we want to quantify the pore-shape homogeneity within a single nanoparticle. Second, we want to compare nanoparticles from the same population to see how consistent the production is. Finally, we would like to quantify the difference between nanoparticles coming from different populations.

To evaluate pore shape variation from the center of the nanoparticle to its natural roughly circular boundary, we mask off several *rings* within the nanoparticle.To compare these sub-populations of pores within the nanoparticle, we need

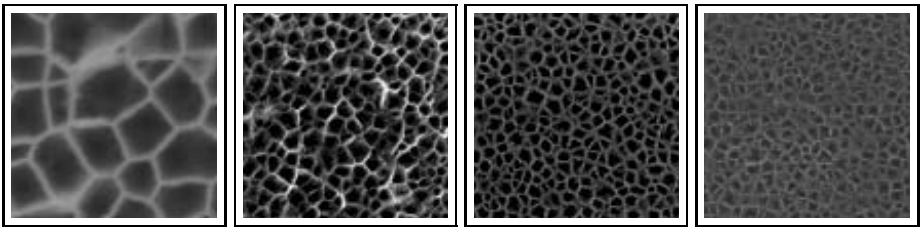

Fig. 4. Several example particles shown with 1:1 pixel dimensions, demonstrating the variability of inputs

Table 1. Estimated values of several features (area, perimeter length, etc.) For pores in the region of interest for several sets of particles. Values are given along with standard error of the mean. The first grouping shows individual sets of similar particles, the three sets in the final grouping are larger collections of particles roughly grouped by size ("Large Pores" LP, and "Extra Large Pores" XLP).

Dataset Name	Long Axis [nm]	Area [nm^2]	Perimeter [nm]	Short Axis [nm]
AG	44 ± 0.18	1100 ± 7.57	100 ± 0.47	34 ± 0.10
AN	75 ± 0.59	3400 ± 47.01	200 ± 1.68	54 ± 0.38
AO	73 ± 0.43	3300 ± 38.71	200 ± 1.32	53 ± 0.32
E18/19	46 ± 0.23	1300 ± 11.07	110 ± 0.63	36 ± 0.14
F2	55 ± 0.80	1800 ± 47.48	140 ± 2.38	40 ± 0.40
F4	55 ± 0.58	1700 ± 26.66	130 ± 1.56	38 ± 0.25
F5	46 ± 0.39	1300 ± 17.79	110 ± 1.11	35 ± 0.23
2 μm	50 ± 0.30	1500 ± 14.53	120 ± 0.83	37 ± 0.19
LP1	51 ± 0.32	1500 ± 15.23	130 ± 0.95	36 ± 0.15
LP2	46 ± 0.13	1300 ± 6.12	110 ± 0.36	35 ± 0.08
XLP1	74 ± 0.32	3400 ± 27.48	200 ± 0.95	54 ± 0.23

to compute robust estimates for the average values of pore shape features over different rings. We first eliminate (and also identify) outliers by quantile analysis on the histograms of pore features values, and thus generate robust estimates of the mean features. Outliers, which are essentially the most oddly shaped pores, can then also displayed for visual inspection by the user.

We have applied our prototype quality control algorithms to SEM imaged samples of various particles production processes. Table 1 collects results from several sets of particles. A typical histogram of three of these features is show in Figure, 5 for one of the data sets.

These results on the statistical distributions of pore characteristics confirms the homogeneity of pore shapes between particles of the same type (i.e generated by the same process). We have studied 8 such groups of between 2 and 4 particles, and within each group, relative variations between particles of mean

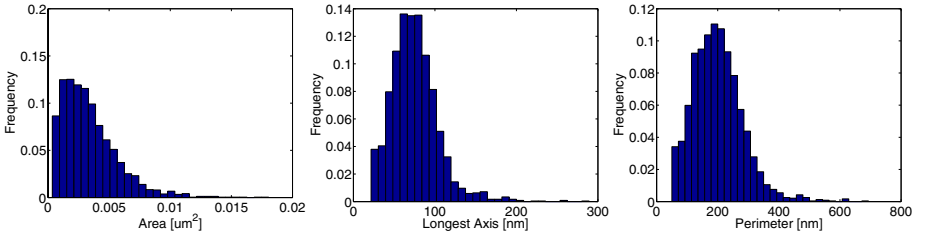

(a) Area (μm^2) (b) Long Axis (nm) (c) Perimeter (nm)

Fig. 5. Relative histograms for three features of the AN set of particles

pore characteristics is small: 5–10% for area, 3–10 % for perimeter, 3–7 % for long axis. The relative accuracy of our estimates of mean pore characteristics for each particle, evaluated by the ratio of standard error over mean, is 0.7–2.5 % for area, 0.5–2 % for perimeter, 0.4–1.4 % for long axis.Thus the accuracy of our estimates is much smaller than the variability between particles of the same type which is a favorable feature for quality control applications.

For difficult SEM images (exhibiting defects such as high oscillations of image intensities, poor adjustment of intensities dynamics, saturation zones, extremely blurred zones) our algorithm still does a very good detection job on 90% of the homogeneous porous area of the particle, and hence the computation of mean pore-shape features remains quite reliable.

For each SEM image of a nanoparticle, roughly 15 seconds of CPU (AMD 4200) are required to generate the tables of mean pore-shape features, the graphic display of pore maps, and the localization of pore outliers. These outputs represent the typical outputs we expect from our future quality control software. Speed of computation could easily be significantly accelerated, since our computing algorithms are highly parallelizable by multi-node treatment

5 Conclusions and Future Research

With these algorithms to analyze individual nanoparticles, we intend to validate our study on a broader collection of SEM images of nanoparticles, to evaluate how processing characteristics during the generation of nanoparticles may or may not affect the pore shapes and pore boundaries. Our research has focused on fast and accurate segmentation/identification of nanopores, combined with extraction of mean pore shapes features and pore homogeneity evaluation. This has immediate applications to specify and implement a future fast and reliable quality control software to monitor quality in nanoparticle production.

References

1. Canham, L.: Bioactive silicon structure fabrication through nanoetching techniques. Adv. Mater. 7, 1033–1037 (1995)
2. Cheng, M., et al.: Nanotechnologies for biomolecular detection and medical diagnostics. Curr. Opin. Chem. Biol. 10, 11–19 (2006)

3. Bayliss, S., et al.: Nature of the silicon-animal cell interface. J. Porus Mater 7, 191–195 (2000)
4. Li, Y., et al.: Polymer replicas of photonic porous silicon for sensing and drug delivery applications. Science 299, 2045–2047 (2003)
5. Buckberry, L., Bayliss, S.: Porous silicon as a biomaterial. Mater World 7, 213–215 (1999)
6. Sun, W., Puzas, J., Sheu, T.J., Fauchet, P.: Porous silicon as a cell interface for bone tissue engineering. Phys. Status Solidi A 204, 1429–1433 (2007)
7. Salonena, J., et al.: Mesoporous silicon microparticles for oral drug delivery: Loading and release of five model drugs. J. Controlled Release 108, 362–374 (2005)
8. Prestidge, C., et al.: Peptide and protein loading into porous silicon wafers. Phys. Status Solidi C 205, 311–315 (2008)
9. Canham, L.: Nanoscale semiconducting silicon as a nutritional food additive. Nanotechnol. 18, 185704 (2007)
10. Foraker, A., et al.: Microfabricated porous silicon particles enhance paracellular delivery of insulin across intestinal caco-2 cell monolayers. Pharm. Res. 20, 110–116 (2003)
11. Decuzzi, P., Lee, S., Bhushan, B., Ferrari, M.: A theoretical model for the margination of particles within blood vessels. Ann. Biomed. Eng. 33, 179–190 (2005)
12. Decuzzi, P., Ferrari, M.: Design maps for nanoparticles targeting the diseased microvasculature. Biomaterials 29, 377–384 (2008)
13. Gentile, F., Ferrari, M., Decuzzi, P.: The transport of nanoparticles in blood vessels: The effect of vessel permeability and blood rheology. Ann. Biomed. Eng. 36, 254–261 (2008)
14. Serda, R., et al.: Porous silicon particles for imaging and therapy of cancer. In: Kumar, C.S. (ed.) Nanomaterials for the Life Sciences. Nanostructured Oxides of Nanomaterials for the Life Sciences, vol. 2, p. 359. Wiley-VCH, Weinheim (2009)
15. Martin, F., et al.: Acute toxicity of intravenously administered microfabricated silicon dioxide drug delivery particles in mice: Preliminary findings. Drugs R D 6, 71 (2005)
16. Tasciotti, E., et al.: Mesoporous silicon particles as a multistage delivery system for imaging and therapeutic applications. Nature 3, 151–157 (2008)
17. Gentile, F., et al.: The effect of shape on the margination dynamics of non-neutrally buoyant particles in two-dimensional shear flows. J. Biomech. (2008)
18. Bouaynaya, N., Schonfeld, D.: Theoretical foundations of spatially-variant mathematical morphology part II: Gray-level images. IEEE Trans. Pattern Analysis Machine Intelligence 30, 837–850 (2008)
19. Soille, P.: Morphological Image Analysis: Principles and Applications, 2nd edn. Springer, Heidelberg (2007)